Future Urban Heat Risk Assessment in Sydney: Integrating Satellite-Derived UTCI with Population Projections

Akihiko Nishino[1,2], Sisi Zlatanova[1], Naohiko Kohtake[2]

[1] School of Built Environment, University of New South Wales, Sydney, NSW 2052, Australia - (a.nishino, s.zlatanova)@unsw.edu.au
[2] Graduate School of System Design and Management, Keio University, Yokohama, Kanagawa, Japan - kohtake@keio.jp

Keywords: Heat Risk, UTCI, Satellite Observation, Population Projection, Spatial Downscaling.

Abstract

Urban heat stress poses an intensifying public health challenge in Australian cities, with Sydney facing increasingly severe summer thermal conditions. We present a reproducible framework for metropolitan-scale future heat risk assessment that integrates satellite-derived Universal Thermal Climate Index (UTCI) with demographic projections to 2031. We define the UTCI-Population Index (UPI), a composite indicator that quantifies population-weighted heat exposure at Travel Zone resolution across Sydney. We implemented two complementary satellite-based approaches: (1) trend-based extrapolation of the GloUTCI-M global UTCI dataset within Google Earth Engine to predict 2031 summer UTCI at 1 km resolution, and (2) a high-resolution spatial downscaling that combines ERA5-HEAT physically consistent UTCI at 28 km with Landsat 8/9 land surface temperature at 30 m, further refined by 3D solar radiation modelling and nine-station BOM bias correction to produce a pedestrian-level UTCI surface. The resulting UPI maps highlight priority zones where high projected thermal stress coincides with large future resident populations, supporting targeted heat adaptation planning. Approach 1 enables long-term metropolitan-scale future projection, while Approach 2 provides more than 30-fold higher spatial resolution for precinct-level intervention design. The two approaches are designed for future integration, with Approach 2's downscaling pipeline applicable to Approach 1's projected UTCI to yield pedestrian-scale 2031 projections; Approach 2 currently serves as a proof-of-concept and does not constitute a direct 2031 high-resolution forecast. The framework is scalable to other Australian and international cities facing growing heat risks under climate change.

1. Introduction

Urban heat stress is an intensifying public health threat in cities worldwide. In Tokyo, heat-illness ambulance dispatches correlate strongly with ambient heat ($r = 0.74$ with WBGT; Nakamura et al., 2022); Phoenix, USA records some of the highest US heat-related mortality (Maricopa County Department of Public Health, 2024); and Athens experienced a prolonged extreme heatwave in 2021 (Founda et al., 2022). Globally, an estimated 489,000 heat-related deaths occur annually (Zhao et al., 2021). In Australia, heat is the leading cause of weather-related mortality, responsible for more cumulative deaths than any other natural hazard (Coates et al., 2014). Sydney, as Australia's largest metropolitan area with over 5.3 million residents, faces significant vulnerability during its summer months (December–February), when high temperatures, humidity, and solar radiation expose millions of people to severe outdoor thermal stress. To reduce heat stress, numerous approaches have been investigated to study cooling of cities (Li et al., 2025; Xu et al., 2025).

The Universal Thermal Climate Index (UTCI; Bröde et al., 2012) is now widely used as the standard metric for outdoor thermal comfort and heat stress assessment. Unlike simpler indices such as the Heat Index or Wet Bulb Globe Temperature (WBGT), UTCI integrates air temperature, humidity, wind speed, and mean radiant temperature (MRT) in a thermophysiological model that reflects the actual thermal load on the human body. UTCI values above 32°C indicate strong heat stress, above 38°C very strong heat stress, and above 46°C extreme heat stress, each associated with significant physiological risks, particularly for vulnerable groups such as the elderly and outdoor workers.

However, characterising thermal stress alone is not sufficient for effective heat risk management. Identifying where heat-stressed populations will be concentrated in the future is essential for translating thermal hazard information into actionable urban planning intelligence: demographic growth patterns determine where interventions such as green infrastructure corridors, cool urban design standards, and heat emergency plans will have the greatest aggregate impact on public health outcomes. A compound risk indicator is therefore needed that integrates spatially distributed UTCI with future population projections, identifying where high thermal stress and large future resident populations simultaneously converge — and thereby enabling evidence-based spatial prioritisation of heat adaptation interventions at metropolitan scale.

Spatially continuous UTCI estimation across Sydney is, however, constrained by the sparse network of Bureau of Meteorology (BOM) ground observation stations. Within the Greater Sydney metropolitan area, only approximately 13 stations provide complete synoptic observations (air temperature, relative humidity, and wind speed) in real time, giving a mean inter-station spacing of more than 20 km. This density is insufficient to capture fine-scale intra-urban thermal variability driven by differences in surface composition, vegetation cover, building geometry, and proximity to water bodies — variability that can exceed 10°C in UTCI across distances of less than 1 km in mixed urban–green environments. Satellite remote sensing offers a means to bridge this gap by providing spatially continuous thermal information at 30 m to 1 km resolution that can be combined with ground observations and physically consistent atmospheric reanalysis products. This study therefore aims to develop a reproducible, satellite-based framework for future metropolitan-scale urban heat risk assessment that integrates spatially distributed UTCI with demographic projections, demonstrated through two complementary remote sensing approaches across the Sydney metropolitan area.

The main contributions of this study are as follows. First, we define the UTCI-Population Index (UPI), a composite indicator incorporating logarithmic population weighting. Second, we implement two complementary satellite-based approaches for spatially continuous UTCI estimation. Third, we integrate 3D solar radiation modelling to improve UTCI estimation. Fourth, we demonstrate that the high-resolution spatial refinement provided by Approach 2 can be further integrated with Approach 1 to enable pedestrian-scale UTCI projection.

2. Related Work

Remote sensing has proven effective for spatially continuous thermal risk assessment at urban scales. Land Surface Temperature (LST) derived from satellite thermal infrared sensors has been widely used to map urban heat islands and quantify spatial thermal variability (Voogt and Oke, 2003). Landsat TM/ETM+/OLI-TIRS provides LST at 30 m spatial resolution with a 16-day revisit cycle (8 days when Landsat 8 and 9 are combined), while MODIS delivers daily imagery at 1 km. These sensors offer complementary trade-offs between spatial resolution and temporal frequency.

UTCI has been increasingly applied in urban outdoor thermal comfort research. Numerical approaches typically derive UTCI from weather station data or urban microclimate models such as ENVI-met, but these approaches are either spatially sparse or computationally intensive at city scale (Tsoka et al., 2018). Yang et al. (2024) developed GloUTCI-M, a global monthly UTCI dataset at 1 km resolution for 2000–2022, generated using a CatBoost machine learning model trained on UTCI values computed from ISD weather station observations. The spatial prediction is driven by satellite-derived covariates including MODIS land surface temperature, nighttime light, land use/land cover, kernel NDVI, and digital elevation model. It is made available through Google Earth Engine (GEE; Google LLC). Di Napoli et al. (2021) produced ERA5-HEAT, a global daily UTCI dataset applying the formal Bröde polynomial to ERA5 reanalysis inputs at approximately 28 km resolution, providing a temporally resolved, physically consistent UTCI baseline. Despite the availability of these global products, spatial downscaling of UTCI from reanalysis to pedestrian-level resolution remains methodologically underdeveloped. Briegel et al. (2025) provide one of the first systematic evaluations of the relationship between satellite LST and pedestrian-level UTCI across urban morphologies, finding a summer Pearson correlation of $r = 0.70$ and identifying the conditions under which LST serves as a reliable proxy for thermal stress. Their framework directly informs the spatialisation coefficient adopted in Approach 2 of this study.

Population-weighted thermal exposure metrics have been developed to translate thermal hazard fields into public health risk indicators. Hu et al. (2019) proposed a methodology for assessing heat exposure in cities by combining spatially distributed temperature data with population distributions. They showed that population-weighting substantially changes risk rankings compared to raw temperature-based assessments. The present study extends this approach by incorporating future population projections and a nonlinear thermal sensitivity function to define the UPI.

Nishino et al. (2026) previously demonstrated ground-satellite fusion for WBGT estimation at event scale by combining weather observations with Landsat LST. They further coupled the thermal field with population density estimated from satellite imagery to produce a heat congestion risk map. The present study extends this prior work to the full Sydney metropolitan scale for Approach 2, replacing the prior BOM-direct UTCI baseline with ERA5-HEAT to achieve better temporal consistency at the afternoon peak heat hour.

3. Data Sources

Four primary data sources were used. (1) GloUTCI-M (Yang et al., 2024): a global monthly UTCI dataset at 1 km spatial resolution for 2000–2022 (methodology described in Section 2). The dataset is distributed as a GEE asset (projects/sat-io/open-datasets/gloutci-m) covering all land areas globally. (2) Landsat 8/9 Collection 2 Level-2 (USGS, 2023): multispectral and thermal infrared imagery at 30 m spatial resolution with a combined effective revisit cycle of approximately 8 days. The thermal infrared sensor (TIRS) provides calibrated land surface temperature estimates after atmospheric and emissivity correction using the USGS LSTE algorithm. (3) BOM Daily Weather Observations (Bureau of Meteorology, 2026): synoptic weather station observations at 15:00 AEDT on 10 January 2026, sourced from the IDCJDW monthly observation reports for each station. We identified 13 Greater Sydney stations with complete records for this date and time, from which nine were selected based on data completeness and spatial coverage: Observatory Hill, Sydney Airport, Sydney Olympic Park, Bankstown Airport, Terrey Hills, Richmond RAAF, Penrith Lakes, Badgerys Creek, and Campbelltown. (4) ERA5-HEAT (Di Napoli et al., 2021): a global daily UTCI dataset produced by applying the Bröde polynomial to ERA5 reanalysis inputs, available as a GEE asset (projects/climate-engine-pro/assets/ce-era5-heat) at approximately 28 km spatial resolution. We used the utci_max band (daily maximum UTCI) for 10 January 2026 as the spatial UTCI baseline for Approach 2.

Demographic data are sourced from the NSW Travel Zone Population Projections 2024 (Transport for NSW, 2024), which provide estimated resident population and employed persons at Travel Zone resolution across New South Wales with projections through 2066. Travel Zones (TZs) are the fundamental spatial units of the NSW Strategic Travel Model, designed by Transport for NSW to represent geographically coherent areas of broadly uniform trip generation and attraction. The current TZ2021 system comprises 4,236 zones across NSW, of which approximately 3,000 cover the Sydney metropolitan area. Zone sizes range from less than 0.1 km² in the inner city to more than 5 km² in outer suburban areas. We used 2031 projected resident population values as the demographic input to the UPI. The rationale for selecting Travel Zones as the spatial unit for UPI aggregation is detailed in Section 4.2. All spatial data were projected to the GDA2020 / MGA Zone 56 coordinate reference system.

4. Methodology

4.1 UTCI-Population Index (UPI) Formulation

We define the UTCI-Population Index (UPI) to quantify population-weighted heat exposure per spatial unit. The index is calculated at the level of NSW Travel Zones — administrative subdivisions used in transport demand modelling and demographic planning across New South Wales. The Sydney metropolitan area encompasses approximately 3,000 Travel Zones, each with 2031 estimated resident population projections from NSW Government planning datasets. UPI for Travel Zone i is defined as:

$$UPI_i = log_{10}(P_i) \times (T_i / T_{ref})^2 \, , \tag{1}$$

where P_i is the 2031 projected resident population of Travel Zone i; T_i is the mean predicted UTCI of zone i (°C); and T_{ref} is the minimum mean UTCI across all zones (21.35°C in this study), serving as the thermal baseline. Its value reflects the spatial minimum across Sydney Travel Zones and will differ in other cities; UPI rank ordering between zones is invariant provided all zones share the same city-wide baseline. Following Hu et al. (2019), who propose a heat exposure index combining population and satellite-derived air temperature as $E_i = \log_{10}(Pws_i) \times (T_i / T_{ref})^2$, our UPI adopts the same bivariate structure applied to a future planning context.

The choice of a logarithmic population weight reflects the orders-of-magnitude variation in resident population across Travel Zones — from a few hundred residents in low-density outer zones to tens of thousands in high-density inner suburbs. A linear weight would allow a single very large zone to dominate the index regardless of its thermal exposure; the logarithm compresses this range while retaining rank ordering, consistent with the principle of diminishing marginal public-health burden at very high densities.

By contrast, temperature varies across Sydney within a single order of magnitude (approximately 26–37°C in summer means), so logarithmic compression is unnecessary and would obscure meaningful thermal contrasts. The squared temperature ratio $(T_i / T_{ref})^2$ serves three purposes: (i) the ratio ensures all values are ≥1, since T_{ref} is the minimum across all zones; (ii) squaring amplifies the contrast between thermally stressed and thermally mild zones; and (iii) normalising against T_{ref} rather than an absolute threshold makes UPI applicable across different climates and seasons without recalibration. Together, these choices produce an index that is sensitive to co-location of large future populations with elevated thermal stress, which is the operationally relevant quantity for long-term heat adaptation planning.

4.2 Spatial Unit: NSW Travel Zones

First, Travel Zones are the native unit of the TZ Population Projections dataset, enabling direct application of 2031 projected resident population without spatial disaggregation or cross-walk to another boundary system. No equivalent future-population product is available at finer spatial granularity across the full metropolitan area. Second, unlike administrative boundaries such as ABS Statistical Area Level 2 (SA2) or Local Government Areas (LGA), Travel Zones are defined by Transport for NSW to capture spatially coherent areas of broadly uniform trip generation and attraction. Zone boundaries are calibrated to local activity concentration: inner-city zones cover as little as 0.1 km², while outer-fringe zones span 5 km² or more, meaning that population counts already encode the relative intensity of local activity. Third, appropriateness of population count over density: we use absolute resident population P_i rather than population density because (i) the variable-size design of Travel Zones means that density conversion would merely reintroduce information already embedded in the zone boundaries, and (ii) population count directly represents the total number of individuals exposed to thermal stress — the operationally relevant quantity for public health resource allocation and emergency planning. This is consistent with Hu et al. (2019). Because the residential base differs from the instantaneous daytime population (which peaks in the CBD), and the 15:00 UTCI represents the worst-case neighbourhood stress level, the UPI should be interpreted as a residential-area heat hazard potential index rather than a count of people simultaneously outdoors.

5. Implementation

This section describes two satellite-based approaches for UTCI estimation that address each other's resolution limitations. Approach 1 achieves temporal depth — a 21-year trend baseline enabling future projection at 1 km metropolitan resolution — but is constrained by the coarse spatial resolution of its GloUTCI-M input (1 km monthly mean), which cannot resolve pedestrian-scale thermal heterogeneity within urban precincts. Approach 2 addresses this spatial limitation by downscaling ERA5-HEAT with Landsat LST to achieve 30 m pedestrian-level resolution, but is currently limited to a single observed extreme heat event day and does not incorporate future projection. Together they form two components of a single framework designed for future integration. In the current study, Approach 1 delivers a predicted 2031 summer mean UTCI surface — a forward projection of the 21-year observed warming trend — that feeds the UPI computation in Section 4.1. Approach 2, by contrast, produces an estimated UTCI surface for a specific observed extreme heat day (10 January 2026), serving as a high-resolution precinct-scale downscaling demonstration rather than a future projection.

5.1 Approach 1: GloUTCI-M-Based Future UTCI Prediction

5.1.1 Data and GEE Processing: We accessed the GloUTCI-M dataset (Yang et al., 2024) via GEE as described in Sections 2 and 3. We extracted the summer months (December, January, and February) for each year from 2001 to 2022 and computed annual summer mean UTCI values per pixel using GEE's image collection averaging functions.

We then performed pixel-wise linear trend analysis using GEE's built-in linear regression capabilities. For each 1 km grid cell, we computed a least-squares linear regression of summer mean UTCI against time (year), yielding slope values in °C/year. The resulting pixel-wise slopes ranged from −0.24 to +0.18 °C/year (mean −0.03, σ = 0.06). To suppress artefacts from noisy time series — particularly anomalous cooling trends at water-body margins — we clipped slopes to the asymmetric range of −0.1 to +0.3 °C/year; the upper bound was not activated by any pixel in the study domain.

5.1.2 2031 UTCI Prediction: The 2031 UTCI prediction was anchored to the 2022 observed summer mean rather than extrapolated from the regression intercept, to avoid the systematic divergence that accumulates when projecting forward from a historical intercept over a multi-decade baseline. The prediction formula is:

$$UTCI_{2031}(x,y) = UTCI_{2022}(x,y) + slope(x,y) \times 9 \; years, \tag{2}$$

This formulation assumes a linear continuation of the trend observed over 2001–2022, which represents a reasonable first-order approximation for decadal-scale urban planning applications but does not account for potential acceleration under high-emission climate scenarios or non-linear feedbacks in urban heat island dynamics. The 9-year extrapolation horizon (2022 to 2031) is sufficiently short to limit compounding uncertainty while providing planning-relevant future projections aligned with available demographic data.

We exported the predicted UTCI raster from GEE to ArcGIS Pro (Esri Inc.) for zonal aggregation. NoData gaps from cloud masking, water body pixels, and sub-pixel zones at the study area boundary were filled using inverse-distance-weighted spatial interpolation. We then computed mean UTCI per Travel Zone using a zonal statistics operation with bilinear resampling.

5.2 Approach 2: ERA5-HEAT × Landsat LST Spatial Downscaling with BOM Bias Correction

5.2.1 ERA5-HEAT × Landsat LST Downscaling: We obtained the daily maximum UTCI (utci_max band) for 10 January 2026 — a peak thermal-stress day selected as the most stringent test of the downscaling method; anticyclonic conditions that produce Sydney heat events characteristically yield cloud-free satellite coverage, making Landsat availability and thermal intensity physically correlated rather than arbitrarily coincident. The ERA5-HEAT data were sourced from Di Napoli et al. (2021) via its public GEE asset (projects/climate-engine-pro/assets/ce-era5-heat). ERA5-HEAT applies the formal Bröde polynomial to ERA5 reanalysis inputs — including 2 m air temperature, dew point, 10 m wind speed, and radiation — providing physically consistent UTCI at approximately 28 km resolution. We combined this with Landsat 8/9 Collection 2 Level-2 LST at 30 m to downscale UTCI to pedestrian-relevant spatial detail using:

$$UTCI\_ERA5\text{-}fine(x,y) = UTCI\_ERA5 + \beta \times (LST(x,y) - LST\_station), \quad (3)$$

5.2.2 Coefficient β Estimation and Solar Radiation Modelling: In the formula above, UTCI_ERA5 denotes the ERA5-HEAT utci_max value extracted from the ERA5 grid cell enclosing Observatory Hill (the single spatial anchor; lon 151.205°E, lat 33.859°S), and LST_station is the Landsat-derived LST averaged within a 500 m buffer around Observatory Hill. Using a single spatial anchor is justified by the small ERA5 spatial variation across Sydney (typically spanning 2–3 grid cells at 28 km resolution), with any residual spatially varying bias absorbed by the subsequent nine-station BOM bias correction (Section 5.2.3). Observatory Hill was selected as the spatial anchor because it is a long-running WMO-standard synoptic station in the central coastal zone of Sydney, providing stable reference conditions less susceptible to the localised inland heat extremes concentrated in the western suburbs.

The spatialisation coefficient β was set to 0.50, representing the approximate slope of the UTCI–LST relationship under summer heat stress conditions in urban environments. Briegel et al. (2025) quantified this relationship for Landsat-derived LST and pedestrian-level UTCI across diverse urban morphologies in a European mid-latitude city, finding a Pearson $r = 0.70$ for summer conditions. Our adopted $\beta = 0.50$ is a physically plausible midpoint value, consistent with the non-linear LST–UTCI relationship documented by Briegel et al. (2025) under heat stress conditions, and is consistent with the conditions of 10 January 2026, which featured clear-sky direct solar radiation, high ambient temperatures (approximately 39–42°C), and low relative humidity across all nine stations — conditions under which the LST–UTCI coupling is strongest. The bias correction anchors the final UTCI surface to observed pedestrian-level thermal conditions regardless of the exact β value; Section 6.4 provides a quantitative sensitivity bound. A spatially uniform β remains an acknowledged simplification: in urban canyons with high building fractions, the LST–UTCI sensitivity may deviate from the adopted value, and morphology-specific β estimation from local multi-station regression is identified as a priority for future work.

Under clear-sky summer conditions such as 10 January 2026, MRT is the dominant driver of UTCI, as it accounts for the combined thermal load from direct solar radiation, diffuse sky radiation, and reflected radiation from surrounding surfaces (Matzarakis et al., 2010). To improve the physical realism of mean radiant temperature (MRT) at each station, we constructed a 2 m resolution Digital Surface Model (DSM) by combining the Copernicus GLO-30 DEM with building heights derived from OpenStreetMap data, processed in ArcGIS Pro. Solar irradiance (GHI) at the nine BOM station locations was estimated using ArcGIS Spatial Analyst AreaSolarRadiation applied to 400 × 400 m DSM patches centred on each station (step5_9stations.py), for the 15:00–16:00 analysis window on day 10 (10 January 2026). Station-level MRT was then estimated using the Thorsson et al. (2007) formula:

$$T\_mrt = T\_air + (\alpha\_k \times f\_p \times GHI) / (4 \times \varepsilon\_p \times \sigma \times (T\_air + 273.15)^3), \quad (4)$$

where $\alpha\_k = 0.70$ (shortwave absorption coefficient), $f\_p = 0.25$ (projected area factor for a standing person), $\varepsilon\_p = 0.97$ (emissivity), and $\sigma = 5.67 \times 10^{-8}$ W m^{-2} K^{-4}. ArcGIS AreaSolarRadiation uses local apparent solar time based on longitude; at Sydney (151°E), this is approximately UTC+10:04, corresponding to AEDT 15:56 — a 56-minute offset from the nominal BOM observation time of 15:00 AEDT. This systematic offset is treated as a methodological limitation (Section 6.3).

5.2.3 BOM Bias Correction: We computed reference UTCI values at each of the nine BOM stations using the Bröde polynomial, with inputs from BOM synoptic observations at 15:00 AEDT on 10 January 2026: air temperature (T_air), dew point temperature derived from relative humidity via the Magnus equation (Alduchov and Eskridge, 1996), wind speed at pedestrian height (1.1 m, corrected logarithmically from the reported 10 m value), and T_mrt from the Thorsson et al. (2007) formula above. Bias at each station was defined as:

$$bias\_i = UTCI\_BOM\_i - UTCI\_ERA5\text{-}fine\_i, \quad (5)$$

Although the Landsat overpass occurs at approximately 10:30 local time while our analysis targets the 15:00 AEDT peak, we do not claim direct temporal substitution: the LST data serve as a spatial redistribution kernel that encodes the relative thermal contrast between surfaces, a pattern preserved under the clear-sky anticyclonic conditions of the study day. The BOM bias correction subsequently anchors the absolute UTCI magnitude to directly observed 15:00 pedestrian-level conditions, mitigating any systematic offset from the overpass time difference. Station biases were spatially interpolated to a continuous field using inverse distance weighting (IDW, power = 2). Although Observatory Hill served as the spatial anchor for the ERA5-HEAT × Landsat LST downscaling step (Equation 3), it returned NoData in the DSM solar radiation extraction due to its coastal location near the raster boundary; its bias was therefore excluded from the IDW interpolation, yielding eight effective bias control points. The final corrected UTCI surface was then computed as:

$$UTCI\_final(x,y) = UTCI\_ERA5\text{-}fine(x,y) + bias\_IDW(x,y), \quad (6)$$

Output values were clipped to 0–55°C, reflecting the physically plausible summer UTCI range in Sydney's climate, where observed values in this study reached a maximum of approximately 51°C; values outside this range were treated as interpolation artefacts in data-sparse fringe areas. This bias correction anchors the downscaled surface to BOM-observed thermal conditions while preserving the spatial variability captured by the ERA5-HEAT × Landsat LST downscaling.

6. Results and Discussion

6.1 Approach 1: Metropolitan Heat Risk Mapping

https://doi.org/10.5194/isprs-annals-XII-4-W2-2026-137-2026

The GloUTCI-M trend analysis across the Sydney metropolitan area revealed spatially heterogeneous warming trends over 2001–2022, with summer mean UTCI rates of approximately +0.1 to +0.2 °C/year in urban and suburban areas. The highest warming rates are concentrated in the western suburbs and the Penrith–Campbelltown corridor, consistent with the intensification of the urban heat island in rapidly urbanising peri-urban growth areas with increasing impervious surface cover. Coastal and harbour-adjacent areas exhibit lower trends, reflecting the buffering effect of maritime air mass incursion. The 2031 UTCI projections indicate summer mean values of approximately 26–37°C across the metropolitan area, corresponding to moderate to very strong heat stress throughout most of western Sydney during peak summer conditions. Under the 2031 projection, approximately 2.24 million residents (39% of the metropolitan total) occupy Travel Zones whose summer-mean UTCI exceeds 32°C (strong heat stress), and 3.37 million (58%) exceed 30°C.

We computed UPI values as defined in Section 4.1 and classified them into five natural-breaks (Jenks) risk categories. The highest-risk zones are concentrated in the central and outer western suburbs — particularly the Cumberland (Merrylands–Guildford), Blacktown, Fairfield, and Bankstown districts — where high projected UTCI, lower tree canopy cover, higher impervious surface fractions, and strong projected population growth under the NSW Government 2031 projections converge, a pattern consistent with known urban heat island distributions in Sydney. This spatial concentration directly supports the prioritisation of urban greening, cool infrastructure, and heat emergency planning in these areas.

Figure 1 visualises UPI as a red-gradient choropleth across Sydney Travel Zones, where deeper red indicates zones where high projected UTCI and large future resident populations are simultaneously concentrated. The gradient encodes this compound risk — the co-occurrence of high thermal stress and large future population — making UPI a more decision-relevant indicator than either thermal hazard or demographic exposure alone.

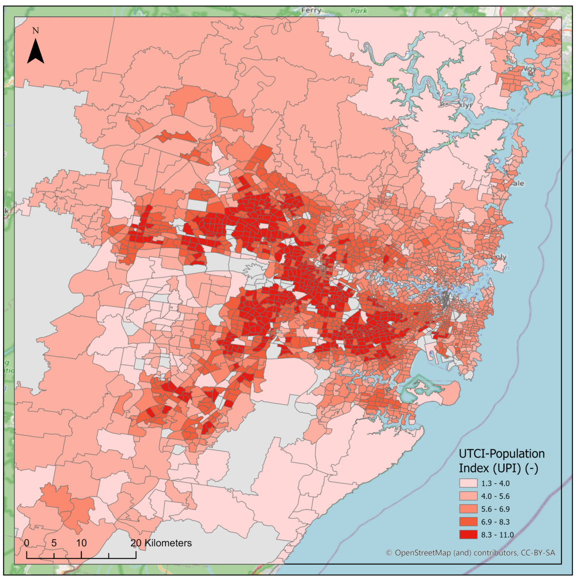

Figure 1. Approach 1 — Predicted UTCI-Population Index (UPI) by Travel Zone for 2031. Natural-breaks (Jenks) classification from Very Low (light) to Very High (dark). Grey zones: non-residential areas (population below 10), excluded. The western Sydney suburbs exhibit the highest UPI values.

For planners, public health administrators, and policy makers, the UPI provides insights unavailable from a UTCI map or a population map alone: the former cannot distinguish thermally extreme but sparsely settled areas from heat-exposed zones with large future populations, while the latter cannot reveal where conditions pose the greatest physiological risk. By integrating both, the classification identifies Travel Zones where high predicted UTCI and strong projected growth converge — precisely where cooling infrastructure, green corridors, cool design standards, and heat emergency planning yield the greatest aggregate public-health benefit. The convergence of high UPI values across these western Sydney suburbs also reveals a structural conflict between demographic expansion and thermal habitability, providing an evidence-based foundation for proactive heat-proofing requirements in precinct planning controls.

For general pedestrians, the UPI map also supports practical heat-aware decisions: timing outdoor activities, selecting routes through lower-risk areas with greater tree canopy, and identifying neighbourhoods served by cool refuges or public drinking water infrastructure. Integrating Approaches 1 and 2 could further enable compound risk-aware applications, such as suggesting cooler, less congested routes during large outdoor events.

6.2 Approach 2: High-Resolution UTCI Mapping

The 30 m UTCI surface for 10 January 2026 showed pronounced intra-urban spatial variability across the Sydney metropolitan area, with estimated UTCI ranging from approximately 29°C in well-vegetated and coastal areas to 51°C in exposed western suburban surfaces — a metropolitan-scale range that is invisible at the 1 km resolution of Approach 1. The ERA5-HEAT × Landsat LST downscaling captured the broad thermal contrast between the cooler eastern coastal zone and the hotter inland west, while the BOM bias correction reduced systematic offset between the ERA5-HEAT baseline and observed surface conditions. In the Sydney CBD, the corrected UTCI surface revealed sharp thermal gradients between sun-exposed plazas (UTCI exceeding 38°C, very strong heat stress) and deeply shaded street canyons, reflecting the influence of building geometry on pedestrian-level thermal comfort. The spatial distribution of the estimated UTCI surface is shown in Figure 2, together with the locations of the nine BOM stations used for bias correction.

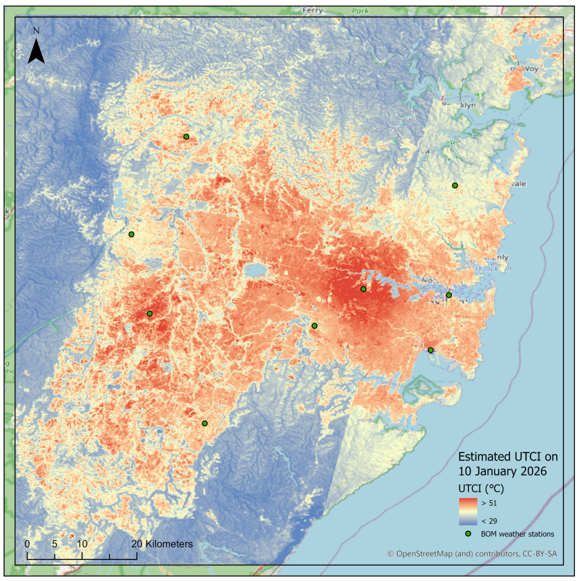

Figure 2. Approach 2 — Estimated UTCI (°C) for 10 January 2026 derived by ERA5-HEAT × Landsat LST spatial downscaling with BOM bias correction (nine stations, IDW

power = 2). Strong intra-urban variability is evident, with UTCI ranging from approximately 29°C in coastal and vegetated areas to 51°C in exposed western suburbs.

Western suburban areas — characterised by open low-density residential morphology, sparse vegetation, and extensive impervious surfaces — displayed the highest UTCI values, with IDW-corrected estimates consistently exceeding 42°C, within the very strong to extreme heat stress range. These patterns are spatially coherent with the Approach 1 UPI risk zones, confirming that the western Sydney suburbs represent the highest-priority area for urban heat adaptation. Vegetated parks and riparian corridors exhibited UTCI values 4–8°C lower than adjacent streets, quantifying the cooling benefit of urban green infrastructure at a scale relevant to precinct-level design decisions. The magnitude of the IDW bias correction ranged from −2.2°C at Penrith Lakes — where ERA5-HEAT overestimated observed thermal conditions — to +3.9°C at Sydney Olympic Park, where the coarse reanalysis underestimated a precinct-scale urban heat island. This 6.1°C range underscores the need for spatially distributed multi-station correction rather than a uniform offset. As these patterns derive from a single extreme-heat day, they demonstrate spatial structure rather than climatological frequency; multi-event validation is identified as future work.

6.3 Methodological Comparison and Limitations

The two approaches serve distinct spatial, temporal, and operational roles within the framework, and are not directly integrated in this study. Approach 1 provides a long-term trend baseline from 21 years of satellite observations and enables future projection, making it suitable for strategic metropolitan-scale planning. However, its 1 km spatial resolution and monthly temporal aggregation limit the analysis of sub-kilometre thermal variability and building-scale effects. Approach 2 provides more than 30-fold finer spatial resolution and captures building-scale thermal patterns by anchoring to a physically consistent UTCI baseline from ERA5-HEAT, but it is limited to specific event dates and does not directly incorporate future projection. Importantly, while LST systematically overestimates UTCI in densely built-up areas by up to 9.7 K in the absence of correction (Briegel et al., 2025), this study mitigates such offsets through nine-station BOM bias correction, anchoring the downscaled surface to pedestrian-level thermal conditions.

Positioned against prior work, the framework occupies a distinct niche. Population-weighted exposure studies (Hu et al., 2019) reorder heat risk rankings but omit future demographic projections and satellite downscaling, whereas the UPI couples projected 2031 populations with a nonlinear thermal-sensitivity term. Relative to LST-based urban heat island mapping (Voogt and Oke, 2003) and computationally intensive microclimate simulation (Tsoka et al., 2018), the present downscaling attains 30 m metropolitan coverage anchored to ERA5-HEAT and ground observations, with an LOO-CV RMSE (2.4°C) comparable to a trained machine-learning emulator (Briegel et al., 2025).

We recommend combining both approaches in the current form: Approach 1 for long-term strategic metropolitan planning and Approach 2 for high-resolution precinct-level intervention design. Looking forward, the most significant methodological opportunity is their full integration: applying Approach 2's ERA5-HEAT × Landsat LST downscaling pipeline to the 2031 UTCI trend projection from Approach 1 would produce a 30 m resolution future UTCI surface — enabling UPI computation at pedestrian scale and substantially increasing the precision of spatial heat risk targeting. Such integration, identified as a primary development goal, would require a future Landsat scene or a statistically downscaled LST projection. It should also be noted that ERA5-HEAT applies the Bröde polynomial directly to ERA5 reanalysis inputs, meaning systematic ERA5 biases (e.g., in wind speed or humidity fields) directly affect its output. GloUTCI-M, by contrast, derives its 1 km spatial variability primarily from satellite-based covariates (MODIS LST and other land surface variables) trained on ISD station observations, although ERA5-Land solar radiation is used in computing the training labels and may partially propagate ERA5 biases into the GloUTCI-M product. For Approach 2, the BOM station bias correction partially decouples the final output from ERA5 by anchoring to ground-observed thermal conditions; no equivalent correction is applied in Approach 1, and ERA5-inherited bias remains a residual uncertainty in the trend projection.

For Approach 2, the ArcGIS AreaSolarRadiation tool uses local apparent solar time; at Sydney (151°E), this creates a 56-minute offset from BOM observation time (15:00 AEDT), introducing systematic timing uncertainty in absolute GHI and MRT estimates that is not currently corrected. A limitation common to both approaches is the assumption of stationarity in the UTCI–LST relationship (Approach 2) and the continuation of historical UTCI trends (Approach 1). In reality, changes in atmospheric moisture, vegetation cover, urban morphology, and local wind regimes under future climate and land-use change may alter these relationships. Future work should incorporate sensitivity analysis of UPI to these non-stationarities and evaluate ensemble-based projections using multiple climate scenario outputs from the CORDEX-Australasia regional climate model archive. Furthermore, the resident population basis of UPI does not capture daytime worker concentrations in the CBD and major employment centres; integration of mobility data or dasymetric disaggregation would improve heat risk identification during peak outdoor exposure hours.

6.4 Accuracy Assessment and Validation

For Approach 1, uncertainty in UTCI estimates arises from ERA5 reanalysis bias in the GloUTCI-M product, the linear trend extrapolation assumption, and the 1 km pixel-to-Travel Zone spatial mismatch in inner-urban areas.

The temporal validity of Approach 1 was evaluated via a pixel-wise hindcast in GEE: linear UTCI trends trained on 2001–2018 GloUTCI-M summer means were projected forward to 2019–2022 and compared against actual observations. Under near-normal climatic conditions (2019–2020), domain-averaged MAE was 0.86°C and 1.24°C respectively, confirming adequate performance of the linear extrapolation. However, 2021 and 2022 showed substantially larger biases (MAE 3.83°C and 4.13°C), coinciding with strong La Niña events that drove anomalous cooling across eastern Australia. These results confirm that linear trend extrapolation captures secular decadal warming adequately under mean-climate conditions but cannot reproduce ENSO-driven interannual variability — a known constraint of trend-based projection methods. For the 2031 UPI projection, this implies the model provides a conservative upper-bound estimate of summer UTCI during strong La Niña phases.

To assess the robustness of these priority rankings to the choice of UPI functional form, we compared three formulations: the adopted (A) $\log_{10}(P) \times (T/T_{ref})^2$, a linear variant (B) $P \times (T/T_{ref})$, and a log-linear variant (C) $\log_{10}(P) \times T$, evaluated across all 2,530 residential Travel Zones. Spearman correlation between the two logarithmic formulations (A and C) was $\rho = 0.98$, with 6 of their 10 highest-ranked zones shared, all within the western Sydney corridor (e.g., Schofields, Guildford West, South Wentworthville, Toongabbie, and Merrylands). The linear-population variant (B) diverged markedly (ρ = 0.70 with A): absolute-population weighting is dominated by the largest zones and strongly down-ranks small-population but thermally extreme zones — Merrylands West (UTCI 36.2°C, population 3,968) falls from rank 5 under A to rank 129 under B, whereas large-population but thermally moderate zones rise to the top. The consistent identification of the western Sydney suburbs as the primary heat-risk concentration across both logarithmic formulations confirms this conclusion is robust to the functional form. This reflects a deliberate design choice: the logarithmic population transform in formulation A prevents large absolute population from dominating the index, ensuring that smaller communities facing extreme thermal stress remain visible to planners.

For Approach 2, the main uncertainties arise from (i) the 28 km spatial resolution of the ERA5-HEAT baseline and its potential bias relative to local urban thermal conditions; (ii) the temporal offset between the Landsat overpass (approximately 10:30 local time) and the 15:00 AEDT reference time, which introduces uncertainty into the LST-based spatial correction; (iii) the 56-minute solar time offset in the AreaSolarRadiation analysis; and (iv) the spatial representativeness of the nine BOM stations for interpolating the IDW bias field across the full metropolitan area.

Cross-validation of the Approach 2 UTCI surface was conducted using a leave-one-out (LOO) procedure across the eight effective BOM stations (Observatory Hill excluded due to NoData in the DSM solar extraction). For each station, the IDW bias field was recomputed excluding that station, and the predicted UTCI was compared with the BOM-derived UTCI_BOM. The LOO-CV yielded a mean absolute error (MAE) of 2.0°C and a root mean square error (RMSE) of 2.4°C (N = 8), with a mean bias of +0.3°C indicating a slight tendency towards overestimation. These errors are comparable to the RMSE of 2.34 K reported by Briegel et al. (2025) for a machine-learning UTCI emulator applied to a European city, and are substantially smaller than the approximately 6°C width separating adjacent UTCI thermal stress categories (bounded at 26, 32, 38, and 46°C), confirming that the bias correction operates within one thermal comfort category at all but one station.

The largest LOO-CV error occurred at Sydney Olympic Park (−5.1°C), which requires interpretation in the context of the full 13-station BOM dataset available for 10 January 2026. Sydney Olympic Park recorded the highest air temperature of any station on that day (T_air = 42.3°C), compared with 40.1–41.9°C at the other seven bias-correction stations and 40.1–40.3°C at the two alternative central-area stations not selected due to spatial redundancy (Canterbury and Horsley Park). Combined with low wind speed (WNW 15 km/h), this produced a UTCI_BOM of 42.91°C at Olympic Park — 3.88°C above the ERA5-HEAT-derived estimate of 39.03°C. The resulting station bias (+3.9°C) was the only positive bias among the eight effective stations; all others ranged from −0.4 to −2.2°C. This configuration is structurally adverse for IDW interpolation: when Olympic Park is excluded from the bias field, the seven remaining negative-bias neighbours produce an interpolated prediction of approximately −1.2°C at that location, diverging from the true +3.9°C bias by 5.1°C.

This outlier reflects a genuine physical mechanism rather than a measurement or processing artefact. ERA5-HEAT, at 28 km spatial resolution, represents UTCI over a grid cell that encompasses not only the Olympic Park precinct but also surrounding residential and industrial areas, producing a spatially smoothed regional thermal estimate that cannot resolve localised hotspots. The Olympic Park precinct — combining sports stadia, sealed plazas, and synthetic surfaces alongside irrigated parklands — generates a precinct-scale urban heat island that coarse reanalysis cannot capture. This resolution limitation is precisely the scientific motivation for the Approach 2 downscaling methodology: the large LOO-CV error at Olympic Park demonstrates in situ that 28 km ERA5-HEAT alone is insufficient to characterise precinct-scale thermal stress, and that high-resolution satellite downscaling combined with station-level bias correction is necessary to resolve such localised urban heat islands. The station was retained in the correction network because its unique positive bias provides the only IDW constraint on the central Sydney bias surface that correctly anchors the corrected UTCI field in this high-exposure precinct.

A bounded sensitivity analysis across $\beta \in \{0.3, 0.5, 0.7\}$ confirmed robustness of the BOM bias correction. Because the spatial correction term $\beta \times$ (LST − LST_station) vanishes at station pixels by construction (LST = LST_station), β affects only the between-station interpolated field. Using representative local LST contrasts ranging from +4.0°C at Sydney Olympic Park to −3.0°C at Terrey Hills, LOO-CV MAE ranged from 1.7 to 2.3°C across $\beta \in \{0.3, 0.5, 0.7\}$ ($\Delta = 0.6$°C), well within the approximately 6°C width of a UTCI thermal stress category.

7. Conclusions

We developed a reproducible framework for future urban heat risk assessment at metropolitan scale, integrating satellite-derived UTCI with demographic projections through the UTCI-Population Index (UPI). We implemented two complementary satellite-based approaches — GloUTCI-M trend extrapolation at 1 km and ERA5-HEAT × Landsat LST spatial downscaling at 30 m with BOM bias correction (the latter serving as a proof-of-concept for the high-resolution spatial refinement module required for future integration with Approach 1) — and demonstrated their practical feasibility across Sydney.

The UPI maps revealed that the highest-risk zones in 2031 are the western Sydney suburbs, where high UTCI and large, growing populations create a converging vulnerability warranting priority attention in heat adaptation planning. Across the eight effective LOO-CV stations, the bias correction achieved an MAE of 2.0°C and an RMSE of 2.4°C, confirming its viability for metropolitan-scale application. The framework relies entirely on publicly available datasets (GloUTCI-M and ERA5-HEAT accessed via Google Earth Engine, Landsat Collection 2, and open-access BOM records) and on transparent, well-documented geoprocessing operations, with no proprietary statistical or machine-learning model dependencies. Several spatial operations in Approach 2 (DSM construction, AreaSolarRadiation, zonal statistics, IDW interpolation) were performed in ArcGIS Pro (Esri Inc.), a commercial GIS, but are replicable with open-source equivalents (GRASS GIS r.sun, QGIS). The UPI should be interpreted as a planning-oriented hazard-exposure prioritisation metric rather than a full epidemiological health risk model: it captures the spatial co-occurrence of projected thermal hazard and future residential population, and does not incorporate individual vulnerability indices or time-varying exposure dynamics.

This framework is scalable and transferable. Comparable implementations are feasible for any Australian capital city and internationally in cities with similar ground observation networks. In the future, we plan to (1) integrate the two approaches by applying Approach 2's ERA5-HEAT × Landsat LST downscaling pipeline to Approach 1's projected 2031 UTCI trend surface, producing a 30 m pedestrian-scale future UTCI field and enabling high-resolution UPI computation; (2) integrate agestratified vulnerability indicators — including elderly population proportions and socioeconomic exposure indices — to develop a comprehensive heat vulnerability index that moves beyond hazard-exposure to full risk characterisation; (3) validate the 30 m UTCI surface through in-situ thermal comfort logger deployments (the current LOO-CV measures only between-station interpolation uncertainty, not absolute accuracy), and extend validation beyond the single-event demonstration to multiple heat-event days using additional Landsat acquisitions; and (4) extend the approach to intra-day UTCI estimation using geostationary satellite data from Himawari-9, enabling near-real-time heat monitoring and integration with operational heat alert systems. These developments are expected to contribute to more effective urban heat risk governance in Australian cities.

Acknowledgements

This study was supported by The Kajima Foundation. The authors thank Transport for NSW for the Travel Zone Population Projections dataset and the Bureau of Meteorology for synoptic observation records.

References

Alduchov, O.A., and Eskridge, R.E., 1996. Improved Magnus form approximation of saturation vapor pressure. *Journal of Applied Meteorology*, 35(4), 601–609. doi.org/10.1175/1520-0450(1996)035%3C0601:IMFAOS%3E2.0.CO;2

Briegel, F., Pinto, J.G., and Christen, A., 2025. Is satellite land surface temperature an appropriate proxy for intra-urban variability of daytime heat stress? *Remote Sensing of Environment*, 331, 115045. doi.org/10.1016/j.rse.2025.115045

Bröde, P., Fiala, D., Błażejczyk, K., Holmér, I., Jendritzky, G., Kampmann, B., Tinz, B., and Havenith, G., 2012. Deriving the operational procedure for the Universal Thermal Climate Index (UTCI). *International Journal of Biometeorology*, 56(3), 481–494. doi.org/10.1007/s00484-011-0454-1

Bureau of Meteorology, 2026. Daily Weather Observations, January 2026. Australian Government. Station IDCJDW monthly reports accessed at www.bom.gov.au/climate/dwo/202601/html/ for nine Greater Sydney stations (see Section 3 for full station list) (4 April 2026).

Coates, L., Haynes, K., O'Brien, J., McAneney, J., and de Oliveira, F.D., 2014. Exploring 167 years of vulnerability: An examination of extreme heat events in Australia 1844–2010. *Environmental Science and Policy*, 42, 33–44. doi.org/10.1016/j.envsci.2014.05.003

Di Napoli, C., Barnard, C., Prudhomme, C., Cloke, H.L., and Pappenberger, F., 2021. ERA5-HEAT: A global gridded historical dataset of human thermal comfort indices from climate reanalysis. *Geoscience Data Journal*, 8(1), 2–10. doi.org/10.1002/gdj3.102

Founda, D., Katavoutas, G., Pierros, F., and Mihalopoulos, N., 2022. The extreme heat wave of summer 2021 in Athens (Greece): Cumulative heat and exposure to heat stress. *Sustainability*, 14(13), 7766. doi.org/10.3390/su14137766

Hu, L., Wilhelmi, O.V., and Uejio, C., 2019. Assessment of heat exposure in cities: Combining the dynamics of temperature and population. *Science of the Total Environment*, 655, 1–12. doi.org/10.1016/j.scitotenv.2018.11.028

Li, J., Zlatanova, S., and Stouffs, R., 2025. Cooling effects of urban green spaces: A systematic review of methods applied in the past two decades. *Sustainable Cities and Society*, 133, 106833. doi.org/10.1016/j.scs.2025.106833

Maricopa County Department of Public Health, 2024. 2023 Heat Related Deaths Report. Maricopa County Department of Public Health, Epidemiology & Informatics. Available at: www.maricopa.gov/1858/Heat-Surveillance (7 April 2026).

Matzarakis, A., Rutz, F., and Mayer, H., 2010. Modelling radiation fluxes in simple and complex environments: basics of the RayMan model. *International Journal of Biometeorology*, 54(2), 131–139. doi.org/10.1007/s00484-009-0261-0

Nakamura, D., Kinoshita, H., Asada, K., Arimitsu, T., Yasumatsu, M., and Ishiwata, T., 2022. Trends in ambulance dispatches related to heat illness from 2010 to 2019: An ecological study. *PLOS ONE*, 17(11), e0275641. doi.org/10.1371/journal.pone.0275641

Nishino, A., Shikida, T., Kodaka, A., Sato, K., Sato, K., Yasunaga, T., Ooba, D., and Kohtake, N., 2026. Combination of WBGT and Pedestrian Flow Estimated based on Satellite Data to Reduce the Heatstroke Risks at Large Outdoor Events. 106th AMS Annual Meeting, 17th Conference on Environment and Health.

Thorsson, S., Lindberg, F., Eliasson, I., and Holmer, B., 2007. Different methods for estimating the mean radiant temperature in an outdoor urban setting. *International Journal of Climatology*, 27(14), 1983–1993. doi.org/10.1002/joc.1537

Transport for NSW, 2024. Travel Zone Population Projections 2024 (TZP24). Transport for NSW Open Data Hub. opendata.transport.nsw.gov.au (4 April 2026).

Tsoka, S., Tsikaloudaki, A., and Theodosiou, T., 2018. Analyzing the ENVI-met microclimate model's performance and assessing cool materials and urban vegetation applications—A review. *Sustainable Cities and Society*, 43, 55–76. doi.org/10.1016/j.scs.2018.08.009

USGS, 2023. *Landsat Collection 2 Level-2 Science Product.* U.S. Geological Survey. doi.org/10.5066/P9OGBGM6.

Voogt, J.A., and Oke, T.R., 2003. Thermal remote sensing of urban climates. *Remote Sensing of Environment*, 86(3), 370–384. doi.org/10.1016/S0034-4257(03)00079-8

Xu, H., Wang, C., Shen, X., Zlatanova, S., and Paolini, R., 2025. Refined definition of level-of-detail for tree models in support of microclimate simulation. *Sustainable Cities and Society*, 126, 106387. doi.org/10.1016/j.scs.2025.106387

Yang, Z., Peng, J., Liu, Y., Jiang, S., Cheng, X., Liu, X., Dong, J., Hua, T., and Yu, X., 2024. GloUTCI-M: a global monthly 1 km Universal Thermal Climate Index dataset from 2000 to 2022. *Earth System Science Data*, 16, 2407–2424. doi.org/10.5194/essd-16-2407-2024

Zhao, Q., Guo, Y., Ye, T., Gasparrini, A., Tong, S., Overcenco, A., Urban, A., Schneider, A., Entezari, A., Vicedo-Cabrera, A.M., et al., 2021. Global, regional, and national burden of mortality associated with non-optimal ambient temperatures from 2000 to 2019: a three-stage modelling study. *The Lancet Planetary Health*, 5(7), e415–e425. doi.org/10.1016/S2542-5196(21)00081-4